

THE OFFICIAL MAGAZINE OF THE OCEANOGRAPHY SOCIETY

# Oceanography

## CITATION

Carbajal, J.C., A.L. Rivas, and C. Chavanne. 2018. High-frequency frontal displacements south of San Jorge Gulf during a tidal cycle near spring and neap phases: Biological implications between tidal states. *Oceanography* 31(4):60–69, <https://doi.org/10.5670/oceanog.2018.411>.

## DOI

<https://doi.org/10.5670/oceanog.2018.411>

## PERMISSIONS

*Oceanography* (ISSN 1042-8275) is published by The Oceanography Society, 1 Research Court, Suite 450, Rockville, MD 20850 USA. ©2018 The Oceanography Society, Inc. Permission is granted for individuals to read, download, copy, distribute, print, search, and link to the full texts of *Oceanography* articles. Figures, tables, and short quotes from the magazine may be republished in scientific books and journals, on websites, and in PhD dissertations at no charge, but the materials must be cited appropriately (e.g., authors, *Oceanography*, volume number, issue number, page number[s], figure number[s], and DOI for the article).

Republication, systemic reproduction, or collective redistribution of any material in *Oceanography* is permitted only with the approval of The Oceanography Society. Please contact Jennifer Ramarui at [info@tos.org](mailto:info@tos.org).

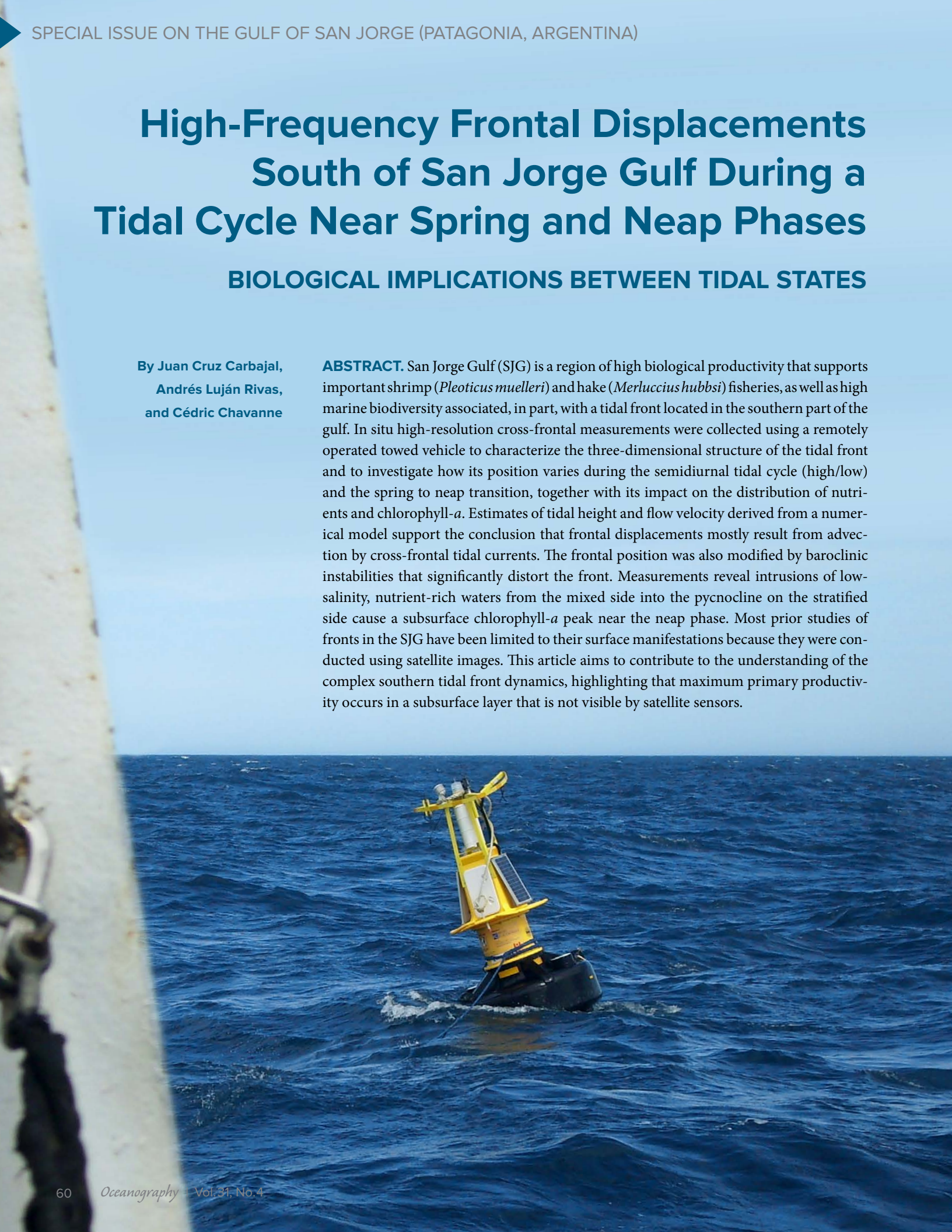
Permission is granted to authors to post their final pdfs, provided by *Oceanography*, on their personal or institutional websites, to deposit those files in their institutional archives, and to share the pdfs on open-access research sharing sites such as ResearchGate and Academia.edu.

# High-Frequency Frontal Displacements South of San Jorge Gulf During a Tidal Cycle Near Spring and Neap Phases

## BIOLOGICAL IMPLICATIONS BETWEEN TIDAL STATES

By Juan Cruz Carbajal,  
Andrés Luján Rivas,  
and Cédric Chavanne

**ABSTRACT.** San Jorge Gulf (SJG) is a region of high biological productivity that supports important shrimp (*Pleoticus muelleri*) and hake (*Merluccius hubbsi*) fisheries, as well as high marine biodiversity associated, in part, with a tidal front located in the southern part of the gulf. In situ high-resolution cross-frontal measurements were collected using a remotely operated towed vehicle to characterize the three-dimensional structure of the tidal front and to investigate how its position varies during the semidiurnal tidal cycle (high/low) and the spring to neap transition, together with its impact on the distribution of nutrients and chlorophyll-*a*. Estimates of tidal height and flow velocity derived from a numerical model support the conclusion that frontal displacements mostly result from advection by cross-frontal tidal currents. The frontal position was also modified by baroclinic instabilities that significantly distort the front. Measurements reveal intrusions of low-salinity, nutrient-rich waters from the mixed side into the pycnocline on the stratified side cause a subsurface chlorophyll-*a* peak near the neap phase. Most prior studies of fronts in the SJG have been limited to their surface manifestations because they were conducted using satellite images. This article aims to contribute to the understanding of the complex southern tidal front dynamics, highlighting that maximum primary productivity occurs in a subsurface layer that is not visible by satellite sensors.



## INTRODUCTION

Fronts in shallow water (Simpson and Pingree, 1978) are formed where bottom-generated turbulence is sufficiently intense to inhibit formation of the seasonal thermocline (Fearnhead, 1975). San Jorge Gulf (SJG; 44.5°–47.5°S, 68°–65°W) has a shallow-water region (45–75 m depth) near 46°48'S, 65°43'W where formation of the seasonal pycnocline is restricted by intense vertical mixing due to high bottom friction (Glorioso and Flather, 1995, 1997; Palma et al., 2004; Tonini et al., 2006; Moreira et al., 2011). In addition, during the Southern Hemisphere warm period (October to March), net surface heat flux is positive (toward the ocean; Rivas, 1994; Rivas and Piola, 2002), sufficient ( $\sim 200 \text{ W m}^{-2}$ ) to warm the surface layer of the SJG and give rise to the southern tidal front (STF).

STF water masses exhibit distinctive hydrographic properties that reflect their origins. The Magellan Plume is a tongue of vertically homogeneous, low-salinity water ( $\sim 33.2$  psu in the southern sector of the gulf) that extends northward to 42°S and comprise the vertically homogeneous portion of the STF. Its source lies in the relatively fresh waters discharged from the Magellan Strait (Palma and Matano, 2012). By contrast, the inner waters of the SJG are influenced by mid-shelf waters (Guerrero and Piola, 1997; Bianchi et al., 2005) that are stratified during the warm period and comprise the vertically stratified portion of the STF water mass.

Traditionally, the stratified region is considered a two-layer system where optimal light and nutrient conditions occur only in the transition zone between the mixed and stratified regions (Le Fevre, 1987). An alternative model has been proposed in which the stratified region operates like a three-layer system (surface, bottom, and middle layers), where horizontal subsurface intrusions of water rich in nutrients may occur, causing subsurface chlorophyll-*a* maxima (Richardson et al., 2000; Matano and Palma, 2018, in this issue).

Most studies of marine fronts on the Patagonian shelf have been conducted using satellite images of sea surface temperature (SST) or chlorophyll-*a* (visible) that only show surface manifestations of fronts (Rivas et al., 2006; Romero et al., 2006; Rivas and Pisoni, 2010; Dogliotti et al., 2014; Pisoni et al., 2015). These studies were also constrained by the availability of images. This article presents the observational results of a program conducted during the austral summer of 2014 in the SJG that was designed specifically to determine the high-frequency variability of the STF. We present the sampling strategy and the numerical model used for the study and describe the methods used to identify the position of the STF. We then demonstrate that frontal displacements are caused by tidal advection associated with different current intensities and that other processes such as baroclinic instabilities modify the shape and location of the front. We also describe the biological impacts triggered by frontal displacements. Finally, we discuss the results of our research and summarize key points.

## MATERIALS

### Study Site and Sampling

Figure 1 presents a synoptic view of the sampling strategy carried out during leg 2 of the MARES (Marine Ecosystem Health of San Jorge Gulf: Present status and Resilience capacity) project to quantify high-frequency displacements of the STF. The observational study was conducted aboard R/V *Coriolis II* and split into three surveys, each consisting of six cross-frontal transects during a nearly complete semidiurnal tidal cycle and different tidal amplitudes (Table 1). During the late spring tide (**1st**) and early neap tide (**ent**) phases, the surveys covered an area of nearly 29.8 km (NW–SE) by 15.1 km (NE–SW) (Figure 1b and 1d, respectively), while in intermediate tide (**it**) phase, the same transect (T1) was repeated six times back and forth (Figure 1c). This article considers only the temporal variability

of the STF during the first (**1st**) and second (**it**) surveys, which lasted 11 h 45 min (tidal amplitude  $\sim 5.3$  m) and 11 h 21 min (tidal amplitude  $\sim 3.2$  m), respectively, because during the third survey, the frontal shape was different from that expected, as will be discussed later.

The data set was acquired with the remotely operated towed vehicle Scanfish II (EIVA Marine Survey Solutions) fitted with a modular CTD (Sea-Bird SBE 49FastCAT) and a combined fluorometer and turbidity sensor (WET Labs model ECO FLNTU). The Scanfish II generates a dense data set that contains between  $6.6 \times 10^4$  and  $2.6 \times 10^5$  values for each variable, depending on transect length (Table 1) and towing speed. Careful quality control/quality assurance of the data set from leg 2 was carried out in order to obtain a database of the highest possible quality (recent work of the authors and M. Charo of the Departamento Oceanografía, Servicio Hidrografía Naval). Because Scanfish II data have non-uniform spacing in both the horizontal and vertical dimensions, the temperature, salinity, density ( $\sigma_t$ ), chlorophyll-*a* (chl), and turbidity calibrated and post-processed data for each transect were interpolated onto a rectangular grid (Table 1). In this article, the high-frequency variability of the STF was analyzed based on the gridded data of each variable.

Additionally, to assess the biological and chemical influence of the front, two southern cross-frontal transects were sampled with a CTD rosette, each consisting of five vertical profiles. The first (Figure 1b) began on February 5 with F1 at 21:28 UTC and ended with F5 on February 6 at 2:35 UTC. The second (Figure 1c) began with F6 on February 8 at 16:26 UTC and ended with F10 on February 8 at 21:28 UTC.

### Hydrodynamic Model

The numerical model used in this study was the MIKE 3 (DHI) 2016 (see <https://www.dhigroup.com/> for further information),



run by Ezcurra & Schmidt SA (<https://www.essa.com.ar/en/>) in hydrodynamic (HD) mode. The model uses a rectangular grid of  $225 \times 265$  nodes that cover the SJG with horizontal and vertical resolutions of 1 km and 5 m, respectively. Tidal amplitudes and phases for the model's open boundaries were obtained from the OSU TPXO model (<http://volkov.oce.orst.edu/tides/global.html>). No atmospheric forcing was used. The tidal height and flow velocities obtained from this model at the grid node  $65^{\circ}54'W$ ,  $46^{\circ}30'S$  (Figure 1a, cyan star) were used to investigate the displacements of the STF in relation to the tidal amplitude and associated currents. The simulation was validated based on sea level predictions for Comodoro Rivadavia and Caleta Paula provided by the Servicio de Hidrografía Naval.

## METHODS

Three methods were used to identify STF shape and position during the cruise period (Table 2).

The horizontal gradient of  $\sigma_t$  was computed by finite differences between consecutive grid points for each transect during 1st and it. Two depths were identified in each of the 12 transects, where the horizontal gradients of  $\sigma_t$  were maximum: one at  $\sim 10$  db associated with the *surface front (sf)* where  $\sigma_t$  increases eastward, and the other at  $\sim 70$  db associated with the *bottom front (bf)* where  $\sigma_t$  increases westward. Table 2 summarizes the positions, times, and magnitudes of the maximum horizontal gradient of  $\sigma_t$  for the *sf* and *bf* during both phases.

The static stability parameter

$$\phi = \frac{g}{h} \int_{-h}^0 (\rho - \bar{\rho}) z dz, \quad \bar{\rho} = \frac{1}{h} \int_{-h}^0 \rho dz,$$

where  $g = 9.81 \text{ m s}^{-2}$  (Simpson and Pingree, 1978), is considered a standardized factor for identifying a marine frontal zone, and represents the amount of energy per unit depth to inject within the system to vertically homogenize a stratified water column with density distribution  $\rho(z)$ . We computed  $\phi$  for each grid column of every transect, and the  $\phi$  values at the positions of the maximum horizontal gradients of  $\sigma_t$  were identified (Table 2). The average of these values was adopted as a critical value ( $\phi_c = 46.4 \text{ J m}^{-3}$ ) to locate the barotropic position of the front (Table 2). Our critical value comes into the range found by other studies (Sabatini et al., 2000, 2004; Sabatini and Martos, 2002; Bianchi et al.,

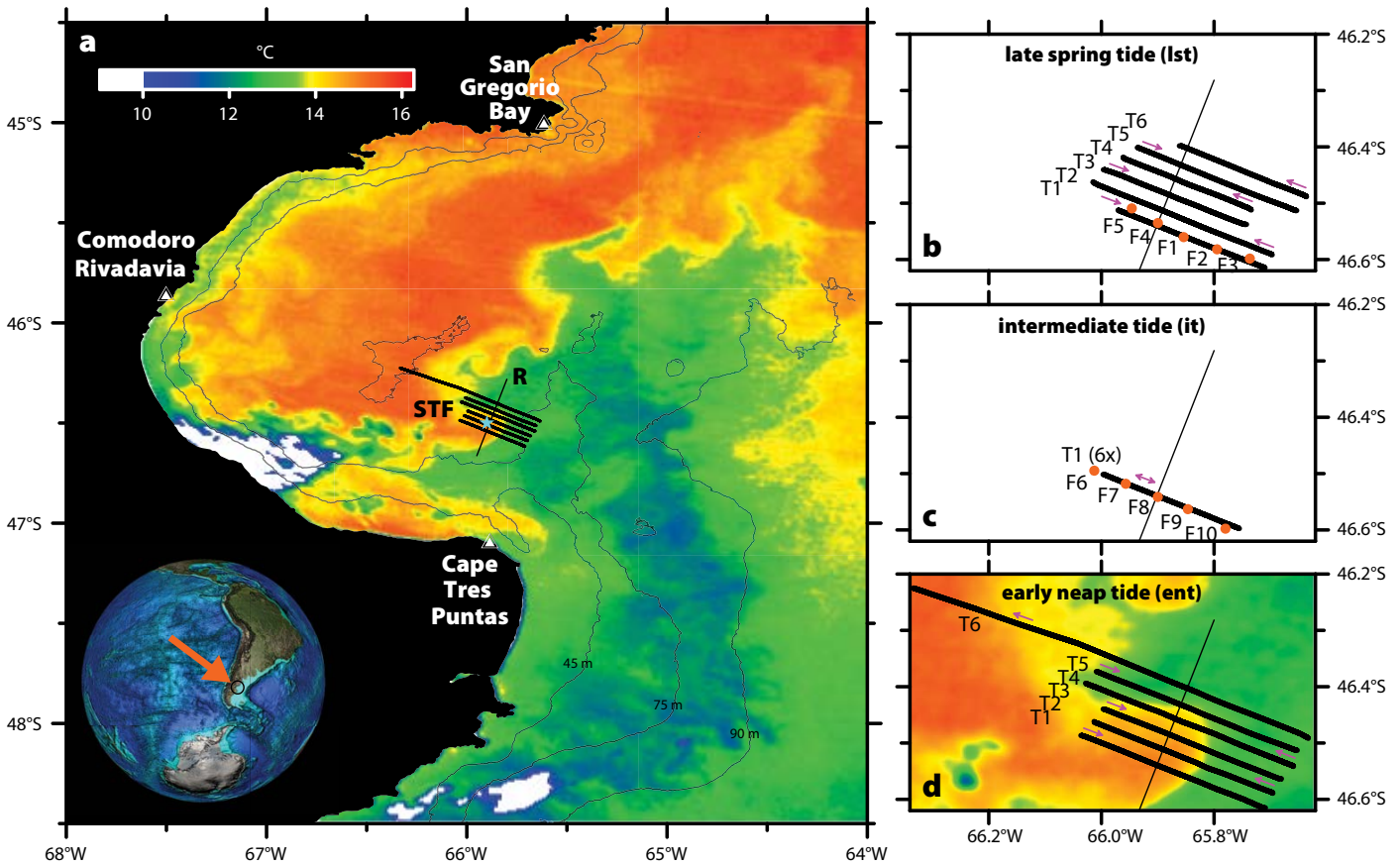


**FIGURE 1.** Study area: The Inset globe (lower left) is a map of South America (from <https://www.ngdc.noaa.gov/mgg/image/images/etopo2v2-modis-globes/>), with the orange arrow indicating the location of San Jorge Gulf. (a) Map showing the Scanfish II transects in the southern tidal front (STF) in San Jorge Gulf for early neap tide (black lines), the arbitrary zero line R perpendicular to the transects (thin black line), and the output node of the numerical model (cyan star). Light black lines are the 45 m, 75 m, and 90 m isobaths. Close-ups of the survey in the southern tidal front for (b) late spring tide, (c) intermediate tide, with locations of CTD rosette vertical profiles shown as orange circles, and (d) early neap tide. Sea surface temperatures from the MODIS sensor on Aqua at 1 km resolution on February 9, 2014, 19:10 to 19:15 UTC are shown as shaded colors (white areas correspond to cloudy regions). Magenta arrows indicate the cruise path. In panel (c), the double arrow alludes to a back and forth survey over transect T1.

2005; Kahl et al., 2017).

Histograms of sea surface temperature images have been used to identify biophysical regions in the ocean (Saraceno et al., 2005). Image pixels are analogous

to grid points of transects in this study. Figure 2 shows histograms of  $\sigma_t$  for **lst** and **it**. The distributions obtained were multimodal for both phases, and three regions were identified associated with the STF:

less dense waters ( $\sigma_t < 24.985 \text{ kg m}^{-3}$  in **lst** and  $\sigma_t < 24.945 \text{ kg m}^{-3}$  in **it**), associated with the surface layer of the vertically stratified side (region 1); intermediate waters ( $24.985 \text{ kg m}^{-3} < \sigma_t$

**TABLE 1.** Field observations in the southern tidal front (STF) accomplished with the remotely operated towed vehicle Scanfish II. Arrows indicate the cruise path parallel to each transect ( $\Rightarrow$  eastward,  $\Leftarrow$  westward). The last two columns show the grid geometry with a resolution of 593–610 m in the horizontal (rows) and 0.6 m in the vertical (columns).  $\Delta x$  represents the transect length. Date and time are reported in Coordinated Universal Time (UTC).

	Transect	Path	Begin		End		Depth Range (m)	$\Delta x$ (km)	Grid Geometry	
			Date (hr:mm)	Lat/Lon (°)	Date (hr:mm)	Lat/Lon (°)			# Columns	# Rows
Late Spring Tide	T1	$\Rightarrow$	Feb 5 (07:38)	-46.512, -65.970	(10:01)	-46.614, -65.709	0.8–79.9	24.0	142	41
	T2	$\Leftarrow$	(10:13)	-46.592, -65.697	(12:10)	-46.462, -66.015	2.4–81.4	28.8	142	48
	T3	$\Rightarrow$	(12:21)	-46.441, -65.996	(13:55)	-46.538, -65.742	2.7–80.0	22.4	142	38
	T4	$\Leftarrow$	(14:08)	-46.512, -65.734	(15:48)	-46.418, -65.961	6.1–80.0	21.2	142	35
	T5	$\Rightarrow$	(15:59)	-46.401, -65.936	(17:43)	-46.513, -65.653	6.8–80.2	25.4	142	42
	T6	$\Leftarrow$	(17:59)	-46.488, -65.636	(19:23)	-46.398, -65.862	4.2–79.7	20.4	142	34
Intermediate Tide	T1-1	$\Rightarrow$	Feb 8 (23:58)	-46.502, -65.997	Feb 9 (01:32)	-46.598, -65.755	0.5–83.0	21.8	142	37
	T1-2	$\Leftarrow$	(01:46)	-46.596, -65.759	(02:55)	-46.518, -65.953	1.5–84.4	17.4	142	30
	T1-3	$\Rightarrow$	(03:05)	-46.518, -65.967	(04:37)	-46.612, -65.720	1.3–82.7	22.1	142	37
	T1-4	$\Leftarrow$	(04:45)	-46.614, -65.710	(06:46)	-46.496, -66.012	2.7–80.7	27.3	142	46
	T1-5	$\Rightarrow$	(07:07)	-46.499, -66.004	(08:45)	-46.612, -65.718	2.7–80.4	25.5	142	42
	T1-6	$\Leftarrow$	(09:00)	-46.615, -65.700	(11:19)	-46.485, -66.036	2.0–85.1	30.4	142	51
Early Neap Tide	T1	$\Rightarrow$	(11:34)	-46.484, -66.036	(13:48)	-46.615, -65.709	4.4–80.2	29.7	142	49
	T2	$\Leftarrow$	(14:02)	-46.589, -65.696	(16:00)	-46.462, -66.013	2.4–80.4	28.6	142	47
	T3	$\Rightarrow$	(16:13)	-46.440, -65.997	(18:06)	-46.563, -65.681	2.7–80.3	28.3	142	47
	T4	$\Leftarrow$	(18:20)	-46.542, -65.659	(21:02)	-46.394, -66.028	2.5–81.5	34.0	142	57
	T5	$\Rightarrow$	(21:17)	-46.373, -66.009	(23:26)	-46.513, -65.652	0.1–80.3	32.0	142	53
	T6	$\Leftarrow$	(23:40)	-46.492, -65.633	Feb 10 (04:13)	-46.225, -66.334	1.7–83.9	63.1	142	105

**TABLE 2.** Summary of the three methods (the horizontal gradient of  $\sigma_t$ , critical static stability parameter  $\phi_c$ , and  $\sigma_t$  distribution local minima) used to identify the position and time of the San Jorge Gulf southern tidal front during late spring tide and intermediate tide phases. The frontal position ( $x$ ) in km and the respective time ( $t$ ) in UTC are shown for the surface front (*sf*) and the bottom front (*bf*), for both the  $\sigma_t$ 's horizontal gradient and the  $\sigma_t$  distribution local minima methods. The magnitude of the density horizontal gradient ( $M$ ) in  $\text{kg m}^{-3} \text{ km}^{-1}$  is also reported with the respective static stability parameter ( $\phi$ ) values.

	Transect	Horizontal gradient of $\sigma_t$ ( $\text{kg m}^{-3} \text{ km}^{-1}$ )								$\phi_c$		$\sigma_t$			
		<i>sf</i>				<i>bf</i>						<i>sf</i>		<i>bf</i>	
		$x$ (km)	$t$ (hr:mm)	$M$	$\phi$ ( $\text{J m}^{-3}$ )	$x$	$t$	$M$	$\phi$	$x$	$t$	$x$	$t$	$x$	$t$
Late Spring Tide	T1	7.80	9:13	0.0555	25.3	7.80	9:13	-0.0990	25.3	6.86	9:09	7.23	9:10	6.89	9:09
	T2	1.10	11:17	0.0403	53.0	1.10	11:17	-0.0747	53.0	1.52	11:16	1.05	11:18	1.46	11:16
	T3	-0.82	13:02	0.0621	63.5	0.38	13:07	-0.0614	45.4	0.28	13:06	-0.69	13:02	3.36	13:19
	T4	0.22	15:06	0.0539	69.0	2.05	14:58	-0.0762	52.1	2.45	14:56	0.45	15:05	5.30	14:42
	T5	6.27	16:52	0.0340	65.9	8.67	17:02	-0.0768	45.7	8.62	17:02	6.80	16:55	11.41	17:14
	T6	6.53	18:51	0.0418	68.5	10.8	18:33	-0.0406	34.7	9.22	18:40	7.91	18:45	–	–
Intermediate Tide	T1-1	7.12	1:05	0.0751	39.3	7.71	1:08	-0.106	27.9	6.57	1:03	7.53	1:07	4.65	0:54
	T1-2	4.88	2:17	0.115	39.8	4.29	2:19	-0.0658	50.1	4.49	2:19	5.05	2:16	1.94	2:29
	T1-3	4.71	3:49	0.0980	30.1	4.20	3:46	-0.0815	43.3	3.97	3:46	5.00	3:50	1.48	3:35
	T1-4	4.18	5:42	0.0774	38.4	3.58	5:48	-0.0798	48.6	3.70	5:44	4.25	5:42	2.64	5:49
	T1-5	6.61	8:07	0.0609	54.0	7.82	8:12	-0.0469	38.8	7.05	8:09	6.96	8:09	7.41	8:10
	T1-6	7.34	9:51	0.0597	50.9	7.34	9:51	-0.0576	50.9	7.64	9:50	7.18	9:52	7.10	9:52

$< 25.275 \text{ kg m}^{-3}$  in **lst** and  $24.945 \text{ kg m}^{-3} < \sigma_t < 25.305 \text{ kg m}^{-3}$  in **it**), associated with the vertically homogeneous side of the front and the intermediate layer (from  $\sim 30$  db to  $\sim 50$  db) of the stratified side (region 2); and relatively more dense water ( $\sigma_t > 25.275 \text{ kg m}^{-3}$  in **lst** and  $\sigma_t > 25.305 \text{ kg m}^{-3}$  in **it**), associated with the bottom layer of the vertically stratified side (region 3). Local minima were identified in the histograms to determine the values of  $\sigma_t$  that delimit the *sf* and *bf* in each tidal phase (Saraceno et al., 2005), and their positions were identified in each transect (Table 2). The water masses of regions 2 and 3 were separated by a more diffuse boundary than that between regions 1 and 2, implying that there was more mixing between regions 2 and 3, as will be discussed later.

Figure 3a (3b) shows vertical sections

of  $\sigma_t$  for **lst** (**it**) together with the frontal positions obtained through the methods detailed above. The black line normal to transects (line R in Figure 1a) sets the arbitrary zero adopted to quantify the front displacements:  $>0$  ( $<0$ ) eastward (westward). The different methods used to determine the frontal position yielded similar results.

## RESULTS

### Frontal Variability

This section aims to quantify the displacements of the STF during a semidiurnal tidal cycle ( $\sim 12$  hours) and a spring to neap transition ( $< 4$  days).

Regardless of the tidal phase, the vertical structure of the STF presents a three-layer system (Figure 3a,b): a well-mixed surface layer that extends up to  $\sim 30$  db containing less dense waters and

bounded below by the *sf* (black lines in Figure 3a,b); an intermediate layer associated with the pycnocline of the STF that reaches  $\sim 50$  db during **it** and  $\sim 35$  db during **lst** and is bounded below by the *bf* (black lines in Figure 3a,b); and finally, a bottom layer of colder and saltier water.

Figure 3c (3d) summarizes the displacements of the *sf* and *bf* during **lst** (**it**) together with the displacements of the water parcels due to the tidal currents along each transect, predicted by the numerical model. Based on  $\phi_c$  values, the barotropic position of the front moved  $\sim 3.9$  km during **it**, while the *sf* and *bf* moved  $\sim 3.2$  km and  $\sim 4.2$  km, respectively. These fronts showed their greatest displacements between transects T1-1/T1-2 and T1-4/T1-5 where the tidal velocity component perpendicular to the front was greater ( $\sim 0.4 \text{ m s}^{-1}$ , in absolute value). Greatest front displacements were also observed between transects T1/T2 and T4/T5 during **lst**, with higher tidal velocities ( $\sim 0.8 \text{ m s}^{-1}$ , in absolute value). In this case, the *bf* moved a greater distance ( $\sim 10.4$  km) than the *sf* ( $\sim 7.3$  km), and the barotropic position of the front moved  $\sim 8.9$  km during the tidal cycle. The STF moved into the interior of the gulf and returned nearly to its position of origin during a semidiurnal tidal cycle and remained nearly motionless during flood/ebb tide. The greater displacements during **lst** leave an area of  $\sim 4$  km where the stability of the water column fluctuates from stratified to well mixed between neap and spring phases, respectively (Figure 3c,d).

In the **ent** phase, the STF was affected by another type of variability. Figure 4 shows the horizontal distribution of  $\sigma_t$ , temperature, and salinity obtained from the shallowest Scanfish II data (surface to 15 db) during that phase. The STF was deformed into an “s-shape,” with a tongue of cold, low-salinity water intruding westward from the homogeneous side of the front, just south of a tongue of warm, saltier water intruding eastward from the stratified side of the front, suggesting a cyclonic circulation (magenta arrows in Figure 4a).

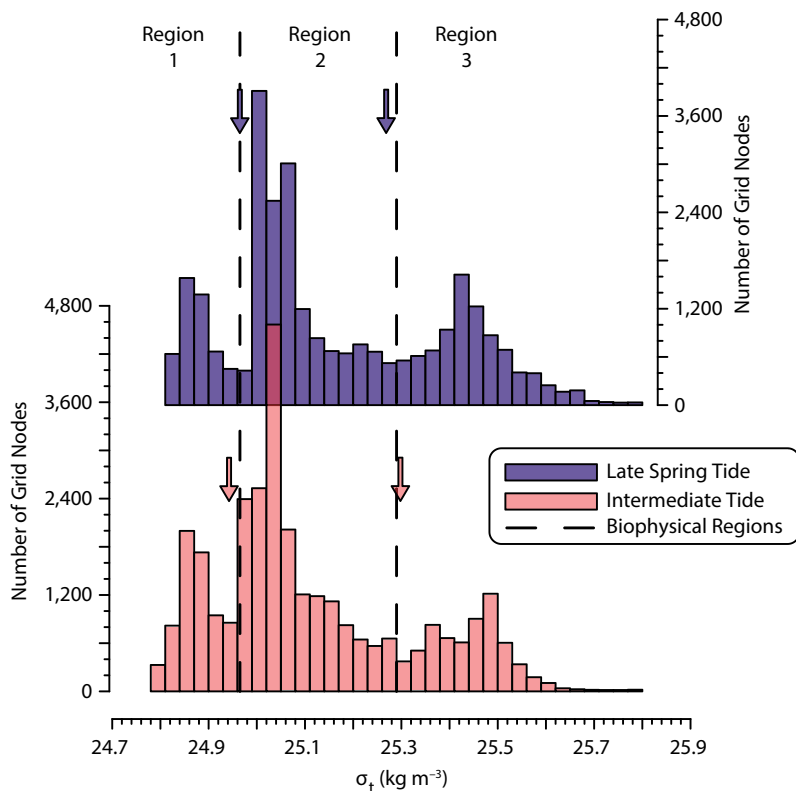


**FIGURE 2.** Histograms of  $\sigma_t$  ( $\text{kg m}^{-3}$ ) for late spring tide (purple columns) and intermediate tide (pink columns) phases. Dashed lines indicate the threshold values of  $\sigma_t$  that separate the biophysical regions of the southern tidal front. On average, region 1 is defined by  $\sigma_t < 24.965 \text{ kg m}^{-3}$ , region 2 by  $24.965 \text{ kg m}^{-3} < \sigma_t < 25.29 \text{ kg m}^{-3}$ , and region 3 by  $\sigma_t > 25.29 \text{ kg m}^{-3}$ . Purple arrows:  $24.985 \text{ kg m}^{-3}$  and  $25.275 \text{ kg m}^{-3}$  are the local minima of the isopycnal distribution that identify the surface and bottom fronts, respectively, for the late spring tide. Pink arrows:  $24.945 \text{ kg m}^{-3}$  and  $25.305 \text{ kg m}^{-3}$  are the local minima of the isopycnal distribution that identify the surface and bottom fronts, respectively, for the intermediate tide.

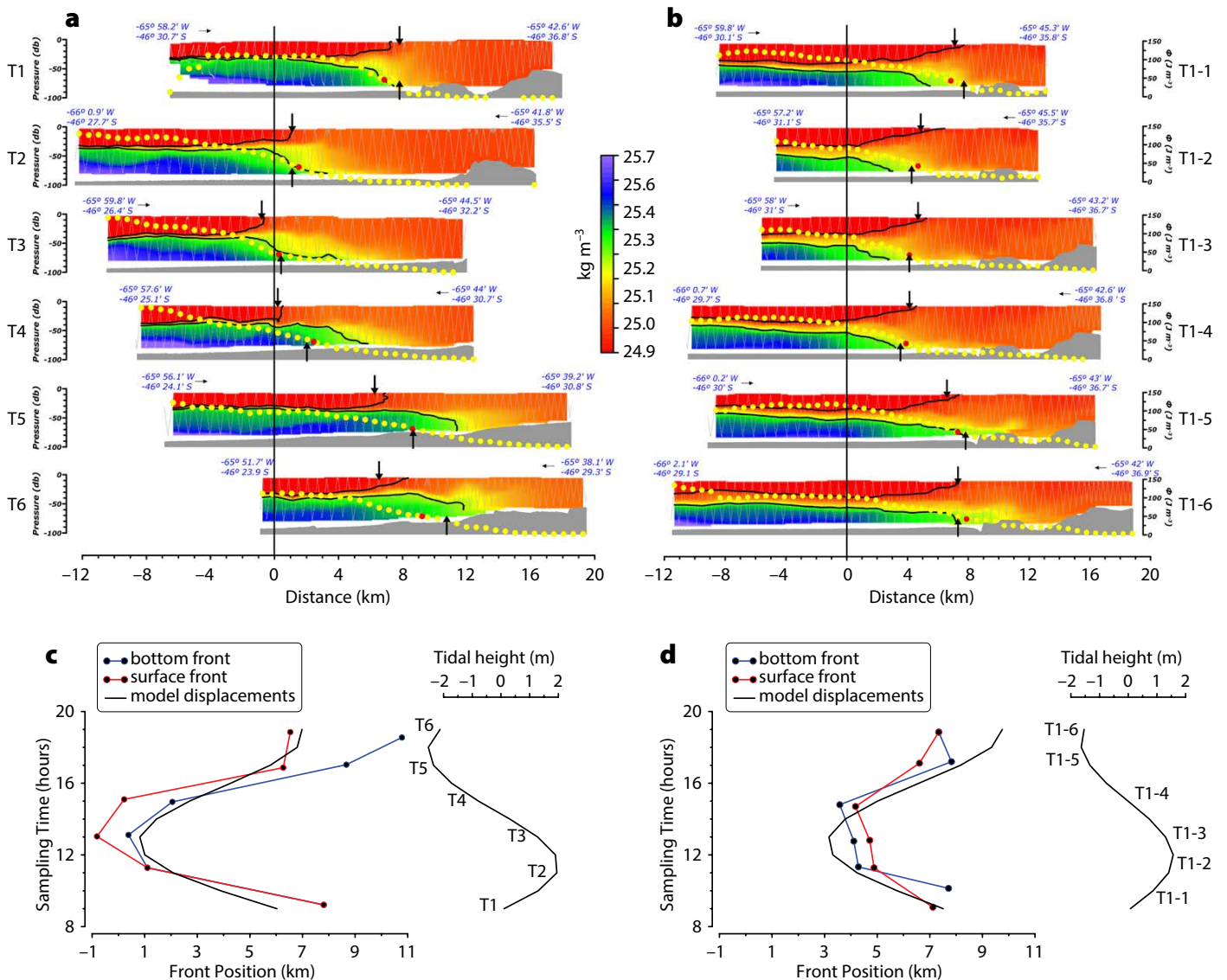
## Biological Implications

Figure 5a,b clearly shows different patterns of the vertical distribution of chl during the two phases in terms of concentration and location in the water column.

During *lst* (Figure 5a) the highest values of chl ( $\sim 0.8 \text{ mg m}^{-3}$ ) were located in the surface layer of the stratified side (between 7 db and 18 db), while in *it* (Figure 5b), the highest values ( $\sim 1.2 \text{ mg m}^{-3}$ ) were located deeper

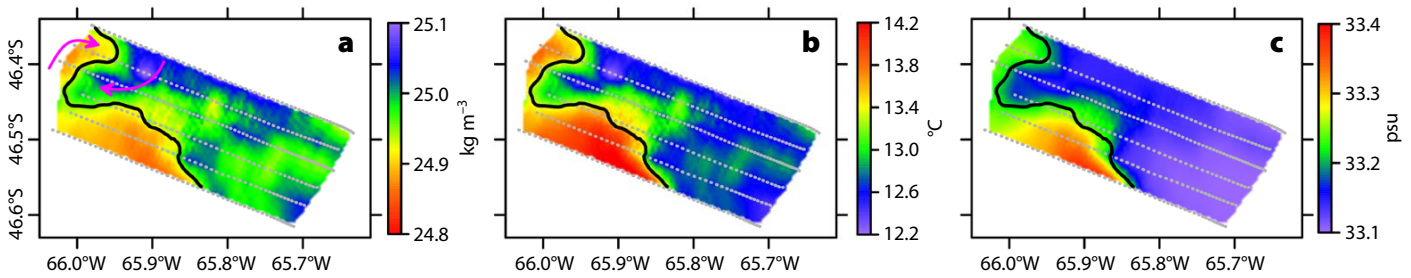
(between 27 db and 39 db), below the *sf*. Note that measurements in *lst* (*it*) were made during the day (at night) (Table 1). Furthermore, the maximum vertically integrated values of chl (*i*-chl) during *it* were greater than during *lst*, and the distance between the frontal position (based on  $\phi_c$ ) and the maximum *i*-chl in each transect remained approximately constant (Figure 5c,d). During *lst*, those distances were greater.

Figure 6a (6b) shows the temperature-salinity (T-S) diagram for transect T1 (T1-1) during *lst* (*it*). This transect was chosen because additional biological and chemical data were available from the rosette water samples and because both transects were conducted during flood tide. Relatively high nutrient values ( $4.1 \mu\text{M}$ ) were found in the homogeneous side of the STF without variation in the water column, while on the stratified side,



**FIGURE 3.** Vertical sections of  $\sigma_t$  ( $\text{kg m}^{-3}$ ) for (a) late spring tide and (b) intermediate tide phases showing in each transect the three methods used for identifying the southern tidal front position. Thick black arrows indicate the locations of the surface and bottom fronts, obtained from the  $\sigma_t$ 's maximum horizontal gradient. Yellow circles indicate the values of  $\phi_c$  for each grid column, and the red circle indicates the critical value of  $\phi$  ( $\phi_c = 46.4 \text{ J m}^{-3}$ ), to identify the barotropic position of the front. Black contours show the isopycnals of (a)  $24.985 \text{ kg m}^{-3}$  and  $25.275 \text{ kg m}^{-3}$  and (b)  $24.945 \text{ kg m}^{-3}$  and  $25.305 \text{ kg m}^{-3}$  that identify the surface and bottom fronts, respectively. The consecutive V-shaped profiles of Scanfish II are marked in light gray, with a dot every five data points, and a black arrow shows the cruise path. The longitude/latitude of transect extremities are shown in blue for each transect. The horizontal scale represents distance in km from an arbitrary zero position (line R in Figure 1a). The profile of the seabed is derived from the ship's EK-60 echosounder. The displacements in km of the  $\sigma_t$ 's maximum gradient for the surface front (bottom front) are shown in red (blue) for (c) late spring tide and (d) intermediate tide. The black line corresponds to the displacement of the water parcel, obtained from the numerical model MIKE 3, for (c) late spring tide and (d) intermediate tide. In addition, the tide height is shown for each phase.





**FIGURE 4.** Horizontal distribution of (a)  $\sigma_t$  ( $\text{kg m}^{-3}$ ), (b) temperature ( $^{\circ}\text{C}$ ), and (c) salinity (psu) in early neap tide. The black contours show the  $24.945 \text{ kg m}^{-3}$  isopycnal that separates surface regions during early neap tide. Magenta arrows in (a) indicate a plausible cyclonic structure. The gray dots mark the data obtained by the Scanfish II from the surface to 15 db.

nutrient values were very high in the bottom layer ( $11.3 \mu\text{M}$ ) and very low in the surface layer ( $0.6 \mu\text{M}$ ), where they have already been consumed.

## DISCUSSION

During both spring and neap phases, the surface layer of the stratified side contains less dense waters influenced by atmospheric conditions, mainly wind stirring and buoyancy fluxes (Simpson, 1971; Simpson and Bowers, 1981). The horizontal contrast between that layer and the adjacent vertically homogeneous waters was not solely thermal. During *it*, a surface salinity gradient of  $-0.12 \text{ psu km}^{-1}$  was observed (salinity decreases eastward at the surface), while in *Ist*, greater variability was found between transects ( $-0.04 \text{ psu km}^{-1}$  to  $-0.12 \text{ psu km}^{-1}$ , not shown). The differences between tidal phases could be linked to different evaporation rates between the front's stratified and homogeneous sides (Badin et al., 2010), or associated with the closer proximity of the STF to the low-salinity tongue of the Magellan Plume during *it* (a weaker tidal flow situates the *sf* into shallower waters during *it*), or associated to along-front variability. Accordingly, the STF acts as a thermohaline front.

Fronts are displaced by the semidiurnal tidal oscillation and the spring-neap cycle (Simpson and Bowers, 1981; Paden et al., 1991; Kasai et al., 1999; Rogachev et al., 2001; Sharples et al., 2007; Hopkins and Polton, 2012). As water enters the gulf with the flood tide, it pushes the front in the west-northwest direction (in the direction of the major axis of the tidal

ellipse; Glorioso and Flather, 1995) and retreats in the opposite direction when the tide ebbs (Figure 3c,d). It seems that frontal displacements are conditioned by tidal amplitude and variability in bottom topography. In comparable conditions of tidal amplitude and bathymetry, Allen et al. (1980) found similar results in a frontal structure at the southern end of the western Irish Sea. The close coincidence between the movement of the fronts and the displacements of the water parcels highlights the dominant impact of tidal advection at these timescales.

We first speculated that the transition zone observed between spring-neap tidal phases (Figure 3c,d) would show a marked biological response, because significant quantities of nutrients from the mixed zone would become trapped in a surface layer with adequate light and thus could be consumed by phytoplankton communities (Loder and Platt, 1985). However, the position of the transition zone and the location of the *i*-chl values were not coincident (Figure 5c,d). It appears that the frontal position changes throughout the tidal cycle as a rigid body, and in addition, those changes occur toward the inside of the gulf during *Ist*.

Shelf sea eddies have been observed in different regions, such as the Celtic Sea (Pingree, 1978; Pingree, 1979), Yellow Sea (Yanagi et al., 1996), Black Sea (Zatsepin et al., 2003), and Oregon shelf waters (Barth et al., 2005), as well as in the California Current System (Castelao et al., 2006). Their typical scale is of the order of a few tens of kilometers, and they persist for some days. In daily images of

SST, they appear as pairs of “hook-like” distortions of the front (Figure 1d). As in Pingree (1978) and Brown et al. (2003), a westward intrusion of cold, low-salinity waters was observed from the homogeneous side of the front just south of an eastward intrusion of warm, saltier waters from the stratified side of the front, suggesting that it could be caused by a cyclonic circulation (Figure 4a). This variability requires further investigation, but it is clear that the survey during *ent* and the few SST images available during the cruise period (Figure 1a) documented the occurrence of eddies in the STF. It is expected that the lateral mixing generated by eddies will have a dynamically significant impact on the location of the front and on the distribution of properties around it.

The combined fluorescence/turbidity sensor incorporated into the Scanfish II enabled us to illustrate the distribution of chl around the STF for different tidal states (Figure 5a,b). The vertical locations of the highest values of chl during *Ist* suggest a balance between light conditions from the surface and nutrient supply from lower layers, while during *it* the deeper location of the highest values could indicate vertical migration of the plankton governed by diurnal variability of light (Anderson, 2001; Villacorte et al., 2015; Flores-Melo et al., 2018, in this issue) associated with the timing of the measurements (Table 1).

During both phases, the *i*-chl maximum was displaced by the same current that advects the front during the quasi-complete tidal cycle, and it was



always located in a region that remains stratified regardless of tidal state and the position of the front (Figure 5b,c). This demonstrates that stratification and turbulence are critical features in the concentration of phytoplankton biomasses (Flores-Melo et al., 2018, in this issue). The maximum values of chl and the maximum of the i-chl during *it* were between 40% and 130% higher than during *lst*, implying that the availability of nutrients was also greater during *it*. This key

observation suggests that some physical processes modulate the nutrient supply to the euphotic zone during the spring-neap cycle. Potential candidates are horizontal intrusion from the mixed region into the surface layer (Holligan et al., 1984), horizontal intrusion from the mixed region into the pycnocline (Pedersen, 1994; Lund-Hansen and Vang, 2004), and vertical upward flux from the bottom layer to the surface layer (Lips et al., 2011). According to the observed

chl distribution, it can be expected that during *lst* (Figure 5a), the vertical fluxes of nutrients were restricted by a sharp pycnocline (Figure 3a), while during *it* (Figure 5b) a weaker pycnocline (Figure 3b) could permit horizontal intrusions from the mixed region into the middle layer of the stratified side. This latter process should be more effective for fertilization judging by the higher concentrations of chl found. Thus, we hypothesize that on the homogeneous

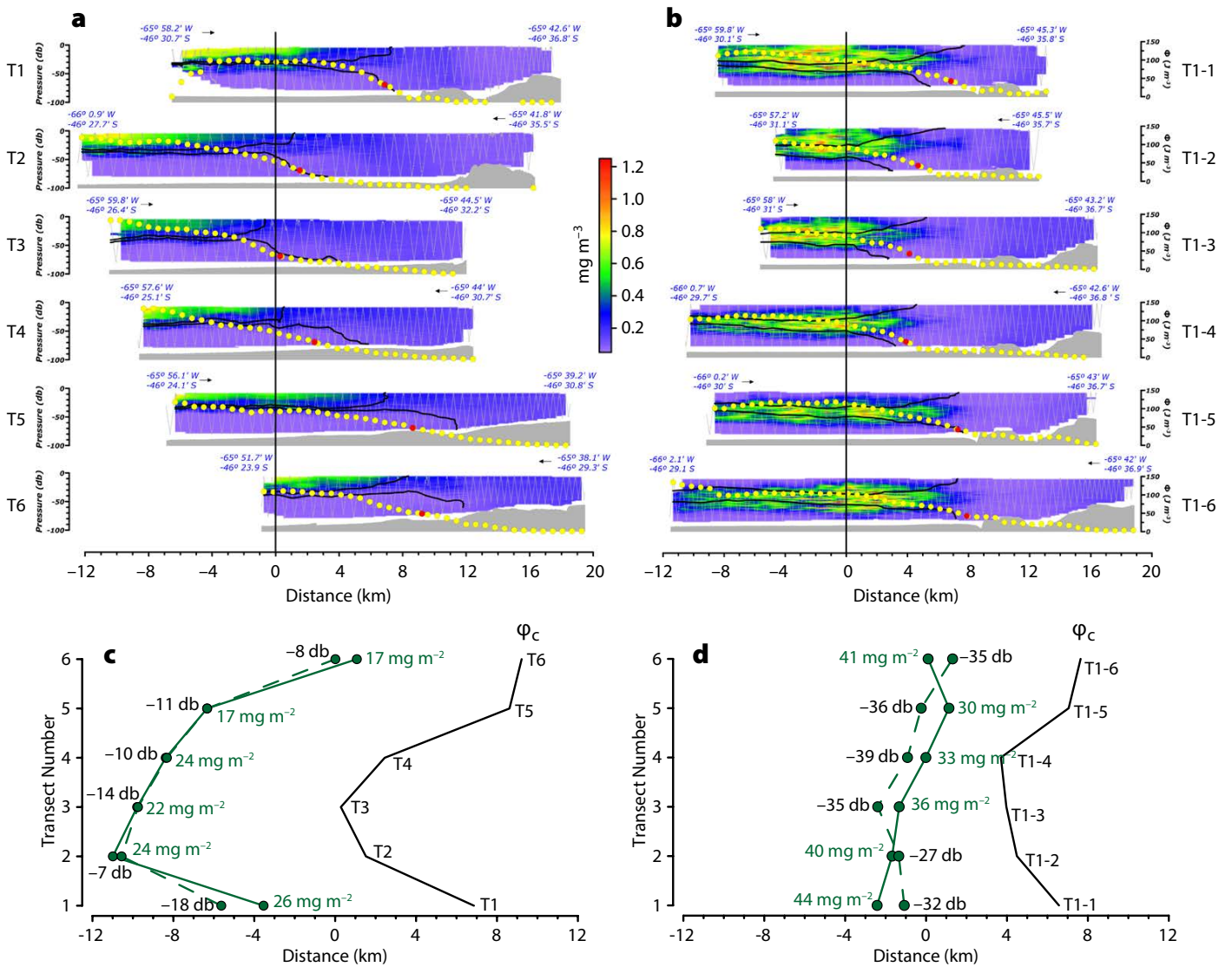


**FIGURE 5.** Vertical sections of chlorophyll (chl in  $\text{mg m}^{-3}$ ) for (a) late spring tide and (b) intermediate tide phases showing in each transect the  $\phi$  values per grid column (yellow circles) and the critical value of  $\phi$ ,  $\phi_c = 46.4 \text{ J m}^{-3}$  (red circle). Black contours show the isopycnals of (a)  $24.985 \text{ kg m}^{-3}$  and  $25.275 \text{ kg m}^{-3}$  and (b)  $24.945 \text{ kg m}^{-3}$  and  $25.305 \text{ kg m}^{-3}$  that identify the surface and bottom fronts, respectively. The consecutive V-shaped profiles obtained by Scanfish II are marked in light gray, with a dot every five data points, and a black arrow shows the cruise path. The longitude/latitude of transect extremities are shown in blue for each transect. The horizontal scale represents distance in km from an arbitrary zero position (line R in Figure 1a). The profile of the seabed is derived from the ship's EK-60 echosounder. The displacements of the maximum vertically integrated values of chl are shown for (c) late spring tide and (d) intermediate tide (green line), highlighting their values in  $\text{mg m}^{-2}$ . The displacements of the absolute maximum values of chl per transect are also shown for (c) late spring tide and (d) intermediate tide (dashed green line), highlighting the depths in db where the maximum has been identified. Also,  $\phi_c$  displacements are shown for each phase (black line).


side, a reduction in light exposure by vertical advection limits primary productivity and, consequently, nutrients remain abundant. On the stratified side, the lack of light in the bottom layer limits consumption, and the availability of light in the surface layer allows nutrients to be nearly totally consumed.

T-S diagrams can provide a useful method for investigating water intrusions (Takeoka et al., 1993). Our T-S diagrams showed similar behaviors during both the *lst* and the *it* (Figure 6). Beneath the *bf*, water masses exhibited two types of mixtures: a deep mixture characterized by a pronounced change of salinity without large differences in temperature (line 1), and a shallower mixture that was warmer and less salty (line 2). Above the *sf*, the mixing occurred between the warm, saline surface waters of the stratified side and the relatively colder, less-salty waters of the vertically homogeneous side (line 3). Finally, between the *sf* and *bf*, the greatest differences and the most interesting behavior were observed. During *it*, we observed mixing between waters of intermediate depths (~40 db) close to the homogeneous side of the front and deep waters of the stratified side (line 4) (Figure 6b). Those waters found

their equilibrium depth in the water column only by cooling ( $\Delta T \approx -2^\circ\text{C}$ ), without a change in salinity (fixed value  $\sim 33.16$  psu), and came from subsurface horizontal intrusion from the mixed region to the middle layer of the stratified side. Moreover, nutrient samples collected during this phase showed concentrations similar to those found on the homogeneous side of the front. Therefore, this process could explain the nutrient supply needed to produce the subsurface chl maximum observed during *it*. During *lst*, such mixing was not observed (Figure 6a), possibly due to the presence of a sharper pycnocline (Figure 3a), which could function as a barrier for the horizontal intrusion.

## SUMMARY

In situ observations acquired with the Scanfish II aboard R/V *Coriolis II* allowed us to obtain the first high spatial and temporal resolution data set in a frontal zone of the Patagonian shelf. These data reveal a dynamically complex three-dimensional frontal structure not accessible from satellite images. Comparison of predictions of tidal height and flow velocity from a numerical model with frontal displacements derived from gridded data

suggest that the STF is advected by the tide as a rigid body during a semidiurnal cycle, independent of the spring-neap phases. The three-layer system identified exhibits a subsurface horizontal intrusion from the mixed region to the pycnocline of the stratified side that is rich in nutrients and that possibly causes the subsurface chl peak observed during the intermediate tide. We speculate that the southern sector of the gulf is being nourished by such intrusions approximately every 15 days. Also, mesoscale variability associated with baroclinic instabilities manifested in the form of meanders of the STF, increasing horizontal mixing and thus lowering the horizontal density gradient. These processes also altered the vertical structure of the front during the early neap phase, and thus they are expected to influence nutrient availability for primary productivity. 

## REFERENCES

- Allen, C., J.H. Simpson, and R.M. Carson. 1980. Structure and variability of shelf sea fronts as observed by an undulating CTD system. *Oceanologica Acta* 3(1):59–68.
- Anderson, D.M. 2001. Phytoplankton Blooms. Pp. 2,179–2,192 in *Encyclopedia of Ocean Sciences*, <https://doi.org/10.1006/rwos.2001.0050>.
- Badin, G., R.G. Williams, and J. Sharples. 2010. Water-mass transformation in the shelf seas. *Journal of Marine Research* 68(2):189–214, <https://doi.org/10.1357/002224010793721442>.
- Barth, J.A., S.D. Pierce, and T.J. Cowles. 2005. Mesoscale structure and its seasonal evolution in the northern California Current System. *Deep Sea Research Part II* 52(1–2):5–28, <https://doi.org/10.1016/j.dsr2.2004.09.026>.
- Bianchi, A.A., L. Bianucci, A.R. Piola, D.R. Pino, I. Schloss, A. Poisson, and C.F. Balestrini. 2005. Vertical stratification and air-sea CO<sub>2</sub> fluxes in the Patagonian shelf. *Journal of Geophysical Research* 110(C7), <https://doi.org/10.1029/2004JC002488>.
- Brown, J., L. Carrillo, L. Fernand, K.J. Horsburgh, A.E. Hill, E.F. Young, and K.J. Medler. 2003. Observations of the physical structure and seasonal jet-like circulation of the Celtic Sea and St. George's Channel of the Irish Sea. *Continental Shelf Research* 23(6):533–561, [https://doi.org/10.1016/S0278-4343\(03\)00008-6](https://doi.org/10.1016/S0278-4343(03)00008-6).
- Castelao, R.M., T.P. Mavor, J.A. Barth, and L.C. Breaker. 2006. Sea surface temperature fronts in the California Current System from geostationary satellite observations. *Journal of Geophysical Research* 111(C9), <https://doi.org/10.1029/2006JC003541>.
- Dogliotti, A.I., V.A. Lutz, and V. Segura. 2014. Estimation of primary production in the southern Argentine continental shelf and shelf-break regions using field and remote sensing data. *Remote Sensing of Environment* 140:497–508, <https://doi.org/10.1016/j.rse.2013.09.021>.
- Fearnhead, P.G. 1975. On the formation of fronts by tidal mixing around the British Isles. *Deep Sea Research and Oceanographic Abstracts* 22(5):311–321, [https://doi.org/10.1016/0011-7471\(75\)90072-8](https://doi.org/10.1016/0011-7471(75)90072-8).

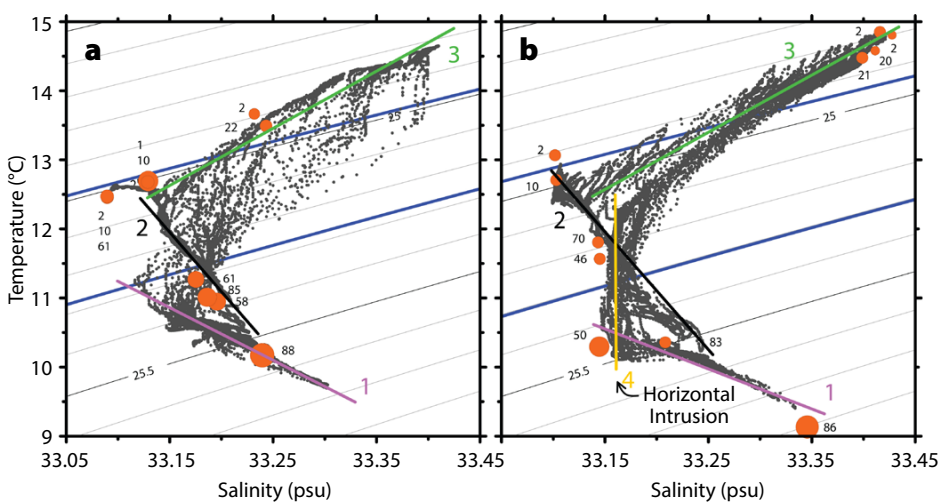


**FIGURE 6.** T-S diagram for transect (a) T1 in late spring tide and (b) T1-1 in intermediate tide. The orange circle sizes indicate the concentrations of nutrients from the water samples, between 0.48  $\mu\text{M}$  and 15.14  $\mu\text{M}$ . The number near each circle indicates the depth in db where the water samples were taken. Blue lines show the isopycnals of (a) 24.985  $\text{kg m}^{-3}$  and 25.275  $\text{kg m}^{-3}$  and (b) 24.945  $\text{kg m}^{-3}$  and 25.305  $\text{kg m}^{-3}$  that identify the surface and bottom fronts, respectively. Contours of  $\sigma_t$  are every 0.1  $\text{kg m}^{-3}$ . The colored lines represent the different water mass mixtures around the front (see text for their characteristics).

- Flores-Melo, X., I.R. Schloss, C. Chavanne, G.O. Almandoz, M. Latorre, and G.A. Ferreyra. 2018. Phytoplankton ecology during a spring-neap tidal cycle in the southern tidal front of San Jorge Gulf, Patagonia. *Oceanography* 31(4):70–80, <https://doi.org/10.5670/oceanog.2018.412>.
- Glorioso, P.D., and R.A. Flather. 1995. A barotropic model of the currents off SE South America. *Journal of Geophysical Research* 100(C7):13,427–13,440, <https://doi.org/10.1029/95JC00942>.
- Glorioso, P.D., and R.A. Flather. 1997. The Patagonian shelf tides. *Progress in Oceanography* 40(1–4):263–283, [https://doi.org/10.1016/S0079-6611\(98\)00004-4](https://doi.org/10.1016/S0079-6611(98)00004-4).
- Guerrero, R.A., and A.R. Piola. 1997. Masas de agua en la plataforma continental. Pp. 107–118 in *El Mar Argentino y sus recursos pesqueros. Antecedentes históricos de las exploraciones en el mar y las características ambientales*, vol. 1. E.E. Boschi, ed., Instituto Nacional de Investigación y Desarrollo Pesquero, Mar del Plata, Argentina.
- Holligan, P.M., P.J.B. Williams, D. Purdie, and R. Harris. 1984. Photosynthesis, respiration and nitrogen supply of plankton populations in stratified, frontal and tidally mixed shelf waters. *Marine Ecology Progress Series* 17:201–213, <https://doi.org/10.3354/meps017201>.
- Hopkins, J., and J.A. Polton. 2012. Scales and structure of frontal adjustment and freshwater export in a region of freshwater influence. *Ocean Dynamics* 62(1):45–62, <https://doi.org/10.1007/s10236-011-0475-7>.
- Kahl, L.C., A.A. Bianchi, A.P. Osiroff, D.R. Pino, and A.R. Piola. 2017. Distribution of sea-air CO<sub>2</sub> fluxes in the Patagonian Sea: Seasonal, biological and thermal effects. *Continental Shelf Research* 143:18–28, <https://doi.org/10.1016/j.csr.2017.05.011>.
- Kasai, A., T.P. Rippeth, and J.H. Simpson. 1999. Density and flow structure in the Clyde Sea front. *Continental Shelf Research* 19(14):1833–1848, [https://doi.org/10.1016/S0278-4343\(99\)00042-4](https://doi.org/10.1016/S0278-4343(99)00042-4).
- Le Fevre, J. 1987. Aspects of the biology of frontal systems. *Advances in Marine Biology* 23:163–299, [https://doi.org/10.1016/S0065-2881\(08\)60109-1](https://doi.org/10.1016/S0065-2881(08)60109-1).
- Lips, U., I. Lips, T. Liblik, V. Kikas, K. Altoja, N. Buhhalko, and N. Rünk. 2011. Vertical dynamics of summer phytoplankton in a stratified estuary (Gulf of Finland, Baltic Sea). *Ocean Dynamics* 61(7):903–915, <https://doi.org/10.1007/s10236-011-0421-8>.
- Loder, J., and T. Platt. 1985. Physical controls on phytoplankton production at tidal fronts. Pp. 3–22 in *Proceedings of the 19th European Marine Biology Symposium*. P.E. Gibbs, ed., Cambridge University Press, Cambridge.
- Lund-Hansen, L.C., and T. Vang. 2004. An inflow and intrusion event in the Little Belt at the North Sea–Baltic Sea transition and a related sub-surface bloom of *Pseudo-nitzschia pseudodelicatissima*. *Estuarine, Coastal and Shelf Science* 59(2):265–276, <https://doi.org/10.1016/j.ecss.2003.09.004>.
- Matano, R.P., and E.D. Palma. 2018. Seasonal variability of the oceanic circulation in the Gulf of San Jorge, Argentina. *Oceanography* 31(4):16–24, <https://doi.org/10.5670/oceanog.2018.402>.
- Moreira, D., C.G. Simonato, and W. Dragani. 2011. Modeling ocean tides and their energetics in the North Patagonia Gulfs of Argentina. *Journal of Coastal Research* 27(1):87–102, <https://doi.org/10.2112/JCOASTRES-D-09-00055.1>.
- Paden, C.A., M.R. Abbott, and C.D. Winant. 1991. Tidal and atmospheric forcing of the upper ocean in the Gulf of California: Part 1. Sea surface temperature variability. *Journal of Geophysical Research* 96(C10):18,337–18,359, <https://doi.org/10.1029/91JC01597>.
- Palma, E.D., and R.P. Matano. 2012. A numerical study of the Magellan Plume. *Journal of Geophysical Research* 117, C05041, <https://doi.org/10.1029/2011JC007750>.
- Palma, E.D., R.P. Matano, and A.R. Piola. 2004. A numerical study of the Southwestern Atlantic Shelf circulation: Barotropic response to tidal and wind forcing. *Journal of Geophysical Research* 109, C08014, <https://doi.org/10.1029/2004JC002315>.
- Pedersen, F.B. 1994. The oceanographic and biological tidal cycle succession in shallow sea fronts in the North Sea and the English Channel. *Estuarine, Coastal and Shelf Science* 38(3):249–269, <https://doi.org/10.1006/ecss.1994.1017>.
- Pingree, R.D. 1978. Cyclonic eddies and cross-frontal mixing. *Journal of the Marine Biological Association of the United Kingdom* 58(4):955–963, <https://doi.org/10.1017/S00253154000456885>.
- Pingree, R.D. 1979. Baroclinic eddies bordering the Celtic Sea in late summer. *Journal of the Marine Biological Association of the United Kingdom* 59(3):689–703, <https://doi.org/10.1017/S0025315400045677>.
- Pisoni, J.P., A.L. Rivas, and A.R. Piola. 2015. On the variability of tidal fronts on a macrotidal continental shelf, Northern Patagonia, Argentina. *Deep Sea Research Part II* 119:61–68, <https://doi.org/10.1016/j.dsr2.2014.01.019>.
- Richardson, K., A.W. Visser, and F.B. Pedersen. 2000. Subsurface phytoplankton blooms fuel pelagic production in the North Sea. *Journal of Plankton Research* 22(9):1,663–1,671, <https://doi.org/10.1093/plankt/22.9.1663>.
- Rivas, A.L. 1994. Spatial variation of the annual cycle of temperature in the Patagonian shelf between 40° and 50° of south latitude. *Continental Shelf Research* 14(13–14):1,539–1,554, [https://doi.org/10.1016/0278-4343\(94\)90089-2](https://doi.org/10.1016/0278-4343(94)90089-2).
- Rivas, A.L., A.I. Dogliotti, and D.A. Gagliardini. 2006. Seasonal variability in satellite-measured surface chlorophyll in the Patagonian Shelf. *Continental Shelf Research* 26(6):703–720, <https://doi.org/10.1016/j.csr.2006.01.013>.
- Rivas, A.L., and A.R. Piola. 2002. Vertical stratification at the shelf off northern Patagonia. *Continental Shelf Research* 22(10):1,549–1,558, [https://doi.org/10.1016/S0278-4343\(02\)00011-0](https://doi.org/10.1016/S0278-4343(02)00011-0).
- Rivas, A.L., and J.P. Pisoni. 2010. Identification, characteristics and seasonal evolution of surface thermal fronts in the Argentinean Continental Shelf. *Journal of Marine Systems* 79(1–2):134–143, <https://doi.org/10.1016/j.jmarsys.2009.07.008>.
- Rogachev, K.A., E.C. Carmack, A.S. Salomatin, and M.G. Alexanina. 2001. Lunar fortnightly modulation of tidal mixing near Kashevarov Bank, Sea of Okhotsk, and its impacts on biota and sea ice. *Progress in Oceanography* 49(1–4):373–390, [https://doi.org/10.1016/S0079-6611\(01\)00031-3](https://doi.org/10.1016/S0079-6611(01)00031-3).
- Romero, S.I., A.R. Piola, M. Charo, and C.A.E. Garcia. 2006. Chlorophyll-a variability off Patagonia based on SeaWiFS data. *Journal of Geophysical Research* 111(C5), <https://doi.org/10.1029/2005JC003244>.
- Sabatini, M., and P. Martos. 2002. Mesozooplankton features in a frontal area off northern Patagonia (Argentina) during spring 1995 and 1998. *Scientia Marina* 66(3):215–232, <https://doi.org/10.3989/scimar.2002.66n3215>.
- Sabatini, M.E., F.C. Ramirez, and P. Martos. 2000. Distribution pattern and population structure of *Calanus australis* Brodsky, 1959 over the southern Patagonian Shelf off Argentina in summer. *ICES Journal of Marine Science* 57(6):1,856–1,866, <https://doi.org/10.1006/jmsc.2000.0969>.
- Sabatini, M., R. Reta, and R. Matano. 2004. Circulation and zooplankton biomass distribution over the southern Patagonian shelf during late summer. *Continental Shelf Research* 24(12):1,359–1,373, <https://doi.org/10.1016/j.csr.2004.03.014>.
- Saraceno, M., C. Provost, and A.R. Piola. 2005. On the relationship between satellite-retrieved surface temperature fronts and chlorophyll *a* in the western South Atlantic. *Journal of Geophysical Research* 110(C11), <https://doi.org/10.1029/2004JC002736>.
- Sharples, J., J.F. Tweddle, J.A. Mattias Green, M.R. Palmer, Y.N. Kim, A.E. Hickman, P.M. Holligan, C.M. Moore, T.P. Rippeth, J.H. Simpson, and V. Krivtsov. 2007. Spring-neap modulation of internal tide mixing and vertical nitrate fluxes at a shelf edge in summer. *Limnology and Oceanography* 52(5):1,735–1,747, <https://doi.org/10.4319/lo.2007.52.5.1735>.
- Simpson, J.H. 1971. Density stratification and microstructure in the western Irish Sea. *Deep Sea Research and Oceanographic Abstracts* 18(3):309–319, [https://doi.org/10.1016/0011-7471\(71\)90036-2](https://doi.org/10.1016/0011-7471(71)90036-2).
- Simpson, J.H., and D. Bowers. 1981. Models of stratification and frontal movement in shelf seas. *Deep Sea Research Part A* 28(7):727–738, [https://doi.org/10.1016/0198-0149\(81\)90132-1](https://doi.org/10.1016/0198-0149(81)90132-1).
- Simpson, J.H., and R.D. Pingree. 1978. Shallow sea fronts produced by tidal stirring. Pp. 29–42 in *Oceanic Fronts in Coastal Processes*. Springer, Berlin, Heidelberg.
- Takeoka, H., O. Matsuda, and T. Yamamoto. 1993. Processes causing the chlorophyll *a* maximum in the tidal front in Iyo-nada, Japan. *Journal of Oceanography* 49(1):57–70, <https://doi.org/10.1007/BF02234009>.
- Tonini, M., E.D. Palma, and A. Rivas. 2006. Modelo de alta resolución de los Golfos Patagónicos. *Mecánica Computacional* 25:1,441–1,460.
- Villacorte, L.O., S.A.A. Tabatabai, D.M. Anderson, G.L. Amy, J.C. Schippers, and M.D. Kennedy. 2015. Seawater reverse osmosis desalination and (harmful) algal blooms. *Desalination* 360:61–80, <https://doi.org/10.1016/j.desal.2015.01.007>.
- Yanagi, T., T. Shimizu, and T. Matsuno. 1996. Baroclinic eddies south of Cheju Island in the East China Sea. *Journal of Oceanography* 52(6):763–769, <https://doi.org/10.1007/BF02239464>.
- Zatsepin, A.G., A.I. Ginzburg, A.G. Kostianoy, V.V. Kremetskiy, V.G. Krivosheya, S.V. Stanichny, and P.M. Poulain. 2003. Observations of Black Sea mesoscale eddies and associated horizontal mixing. *Journal of Geophysical Research* 108(C8), <https://doi.org/10.1029/2002JC001390>.

## ACKNOWLEDGMENTS

This research was supported by an agreement between Argentina and Canada within the framework “Pampa Azul” through the Ministry of Science and Technology (MINCYT) and the Université du Québec à Rimouski (UQAR), respectively. We are grateful to the crew of R/V *Coriolis II* and the Institut des Sciences de la Mer de Rimouski (ISMER). The authors also wish to thank Gabriel Danielli from Ezcurra & Schmidt SA for providing the data from the numerical model.

## AUTHORS

**Juan Cruz Carbajal** (carbajaljuancruz@gmail.com) is a PhD candidate, Centro para el Estudio de Sistemas Marinos-Consejo Nacional de Investigaciones Científicas y Técnicas (CESIMAR-CONICET), Puerto Madryn, Chubut, Argentina. **Andrés Luján Rivas** is an independent researcher, CESIMAR-CONICET, Puerto Madryn, Chubut, Argentina. **Cédric Chavanne** is Professor, Institut des Sciences de la Mer de Rimouski, Université du Québec à Rimouski, Québec, Canada.

## ARTICLE CITATION

Carbajal, J.C., A.L. Rivas, and C. Chavanne. 2018. High-frequency frontal displacements south of San Jorge Gulf during a tidal cycle near spring and neap phases: Biological implications between tidal states. *Oceanography* 31(4):60–69, <https://doi.org/10.5670/oceanog.2018.411>.